Assessment of Modeling and Discretization Accuracy for High-Speed Afterbody Flows

Robert E. Childs* and Steven C. Caruso*
Nielsen Engineering & Research, Inc., Mountain View, California 94043

The accuracy of Reynolds-averaged Navier-Stokes calculations of axisymmetric high-speed afterbody flows is investigated. An approximate truncation error analysis is used to identify specific regions where discretization errors are large, and grid refinement is used to evaluate global solution accuracy. Good alignment of grid lines with streamlines in the shear layer at the nozzle exit is found to be important for obtaining solutions at high nozzle pressure ratios. Solution-adapted grids are used, and solutions that are essentially grid-independent are obtained. Modifications to the $k-\varepsilon$ model for Mach number and streamline curvature effects are presented and validated in flows unrelated to base flows. In base flow calculations, these model modifications produce changes in base drag in excess of 20%. Computed solutions agree well with experiment for base pressure and flow structure.

Nomenclature

a = sound speed
C = turbulence modeling coefficient
h = distance between grid nodes
k = turbulence kinetic energy per unit mass
L = symbolic representation of governing equation
M = Mach number, U/a
NPR = nozzle pressure ratio, p_j/p_∞
p = pressure
P_k = rate of production of ρk in Eqs. (6) and (7)
q = flow variables
Re = Reynolds number
U,V = mean velocities
x,r = spatial coordinates, normalized by body radius
δ = shear layer thickness
δ_{ij} = Kronecker delta
ε = rate of dissipation of k per unit mass
μ = viscosity
ρ = density
σ = model coefficients
τ_{ij} = stress tensor

Subscripts
h = associated with grid spacing h
j = nozzle exit conditions
t = turbulent
∞ = freestream conditions

Model Designations
STD = standard $k-\varepsilon$ model, Eqs. (5–7)
M = with Mach number modification, Eq. (8)
C = with curvature modification, Eqs. (9–11)
MC = with both M and C modifications

Introduction

FLOW in the afterbody region is important to the performance of many flight vehicles, including missiles, ordnance projectiles, space launch vehicles, and aircraft. Drag, stability, surface heating, infrared signature, and noise generation are affected by the afterbody flow. A typical afterbody region of a tactical missile, sketched in Fig. 1, involves an external flow, which may be subsonic or supersonic, a supersonic propulsive jet, and a complex pattern of shocks, expansions, and shear layers. Flow reversal occurs behind the bluff afterbody and may occur on the body if there is a boattail or a large plume.

Methods for estimating the characteristics of afterbody flows are needed for design and analysis purposes. Various types of prediction methods, including component models,[1] methods based on viscous-inviscid interaction,[2] and Euler equation methods, have been used over the past few decades. At present, it is feasible to use prediction methods that solve the Reynolds-averaged Navier-Stokes equations for axisymmetric and three-dimensional flows. Computational methods based on the Navier-Stokes equations were first applied to afterbody flows during the 1970's (e.g., Holst,[3] Mikhail[4]). During the early 1980s, Deiwert et al.[5] employed the Beam-Warming algorithm[6] to compute a variety of afterbody flows, including ones with propulsive jets. Solution-adapted grids were used to obtain good resolution of shocks and shear layers, and the Baldwin-Lomax model was used to predict turbulent stresses. Sahu and Nietubicz[7] used a similar computational method to investigate a variety of projectile flows and reported reasonably good accuracy. Lombard et al.[8] and Hoffman et al.[9] employed different numerical algorithms and grid procedures for afterbody flows. Thomas et al.[10] used the Beam-Warming algorithm and the $k-W$[11] and $k-\varepsilon$[12] turbulence models to predict an axisymmetric base flow with a propulsive jet; significant differences were noted in the results given by the two models.

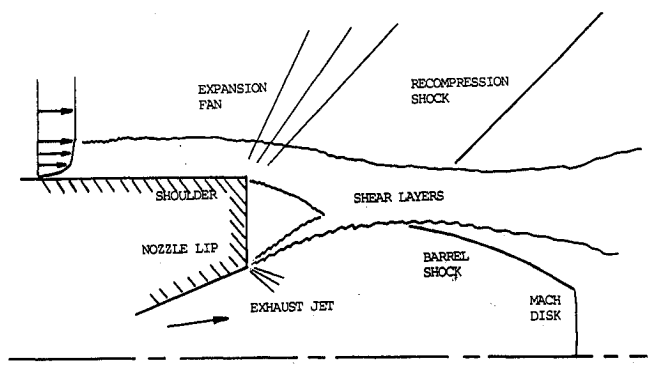

Fig. 1 Sketch of flow in missile afterbody region.

Presented as Paper 89-0531 at the AIAA 27th Aerospace Sciences Meeting, Reno, NV, Jan. 9–12, 1989; received Feb. 20, 1989; revision received July 2, 1990; accepted for publication July 9, 1990.

*Research Scientist. Member AIAA

Some persistent problems can be identified in previous calculations. The flow near the edge of the nozzle exit of underexpanded jets undergoes a rapid expansion and turning as it exits the nozzle, and it is difficult to compute accurately. Many methods predict an "undershoot" in the pressure which can produce negative pressures at moderate *NPR* and terminate the calculation. Fox[13] and Deiwert et al.[5] circumvented this problem by imposing nozzle exit boundary conditions a short distance downstream of the actual exit, where the scale of the flow gradients was large enough to resolve without excessive grid clustering. Venkatapathy and Lombard[14] used a grid-imbedding technique to cluster many points in these regions; however, the undershoot in pressure still existed. Many calculations, including the present ones, employ the questionable assumption of idealized flow within the exhaust nozzle. Computing the internal flow in addition to the external flow has been shown to give a more accurate base pressure[14] than is obtained by assuming idealized flow in the nozzle.

The inability to obtain reliably accurate predictions of flows involving separation is another persistent problem. Several types of flow-prediction methods were evaluated by Putnam and Bissinger[15] for a range of afterbody configurations and operating conditions. They noted that most procedures, from component methods to Navier-Stokes solvers, could predict trends, but flow details were often significantly in error. Navier-Stokes methods were generally inaccurate downstream of separation. Petrie and Walker[16] performed a blind-test evaluation of several Navier-Stokes and component methods for a bluff-based missile afterbody flow with a small propulsive jet. Base pressures were predicted very poorly by the Navier-Stokes methods, and nominally similar methods gave quite different results. Much of the inaccuracy was attributed to discretization errors, and recent results[9,14,17,18] on finer grids were more accurate than the initial results. However, these results did not demonstrate that the grid-independent solutions agreed well with experiment.

Turbulence modeling may also introduce serious errors in many afterbody flow calculations. Numerous phenomena that occur in these flows are known[19] to be represented poorly by commonly used models. Among these are nonequilibrium effects due to transitions between attached, free, and merging shear layers, the effects of high Mach number, shocks, streamline curvature, strong pressure gradients, and density gradients. For example, a 250% increase in shear stress specifically due to curvature effects is predicted by Bradshaw's[20] model in some regions of the $NPR = 2.15$ case reported by Petrie and Walker.[16] Mach-number effects are expected to reduce shear stresses by roughly 75% in other regions. Effects of this magnitude cannot be disregarded in a comprehensive model for turbulence in high-speed afterbody flows.

The present study focuses on turbulence modeling and discretization errors. Errors due to the modeling of turbulence cannot be assessed other than by referring to experimental data, nor can they be reduced easily. The errors introduced when the governing equations are discretized and solved on a numerical grid can be analyzed and can be reduced by using higher-accuracy numerical methods or finer computational grids. The goals of this work are to identify discretization and turbulence modeling errors and to demonstrate means of reducing or eliminating these errors.

The afterbody flow experiments reported by Petrie and Walker[16] are used for comparison with most calculations reported herein. The afterbody configuration and flowfield are similar to that shown in Fig. 1. The test model consisted of a strut-mounted tangent-ogive cylinder that was 18-body radii long and had a bluff base. The model had a centered $M = 2.7$ conical nozzle with a 10 deg half-angle and a nozzle exit radius of 0.2 body radii. The exhaust jet had the same stagnation temperature as the freestream. The freestream conditions were $M_\infty = 1.4$ and $Re_\infty = 64000$, based on body radius. Measurements were reported at $NPR = 2.15$ and 6.44. The external boundary layer was measured 3.2 radii upstream of the base; inflow boundary conditions were prescribed at this location and at the nozzle exit plane.

The implicit finite-volume method and computer code TURF developed by Coakley[21] were used in the present work. Inviscid fluxes are computed with a second-order characteristic scheme. Second-order central differencing is used for the viscous terms in both spatial directions. The flow is predominantly supersonic at flow-through boundaries, and numerical boundary conditions there are straightforward. The $k-\varepsilon$ turbulence model, with and without modifications, is used for all results presented here. This model and the modifications to it are discussed below.

Two solution-adapted grid methods, an algebraic scheme based on the concept of control points (e.g., Ref. 22) and a hyperbolic method,[23] were used. Grid lines are clustered to resolve the shear layers so that shear stresses are computed by a turbulence model rather than by "numerical viscosity." However, shocks in nonreacting gases are captured over a few grid points and do not require special grid clustering. Grids were manually adapted to the flows. The far-field boundaries were sufficiently remote to insulate the afterbody region from their effects. A typical grid and solution are shown in Fig. 2.

Discretization Accuracy

Inaccuracies associated with the discretization of the Navier-Stokes equations on a computational grid can cause large errors in afterbody calculations. Global solution characteristics can depend strongly on the grid,[8,14,16] and the undershoot in pressure at the nozzle exit can prevent convergence. Truncation errors, from truncated series expansions in differencing or interpolation procedures, are the source of these errors.

The Navier-Stokes equations consist of terms such as $\partial F/\partial x$, in which F is a flux of mass, momentum, or energy. Truncation error is the difference between the analytic value and the discrete approximation of $\delta F/\delta x$, and it is greatest where F has significant higher derivatives. Fluxes are continuous along streamlines due to inviscid conservation-law mechanisms, while normal to streamlines, fluxes are continuous due to diffusion. Hence, the flux gradients normal to streamlines can be much greater than streamwise gradients in shear layers. However, the convective flux normal to streamlines are zero, because there is no velocity component in that direction, and other streamline-normal fluxes are often small, as well. Aligning the grid lines with streamlines reduces the truncation error because 1) the streamwise fluxes vary slowly and gradients can be computed accurately, and 2) the streamline-normal fluxes are generally small so that the absolute error in the calculation of their gradients is also small. Aligning grid lines with streamlines significantly reduces the truncation error in Navier-Stokes calculations.

A method based on Richardson extrapolation[24] for estimating the truncation error is outlined below and used to quantify the truncation error in a base-flow calculation. The flow equations are expressed in operator form as

$$L(q) = 0 \tag{1}$$

in which q is the exact solution of the flow equations. The discretized equations, retaining the dominant error term, are

$$L_h(q) + h^n E(q) = 0 \tag{2}$$

in which h is the grid spacing, $h^n E$ is the truncation error, and n is the order of accuracy of the discretization ($n = 2$ for a second-order method). Doubling the grid spacing from h to $2h$ yields the following equation:

$$L_{2h}(q) + (2h)^n E(q) = 0 \tag{3}$$

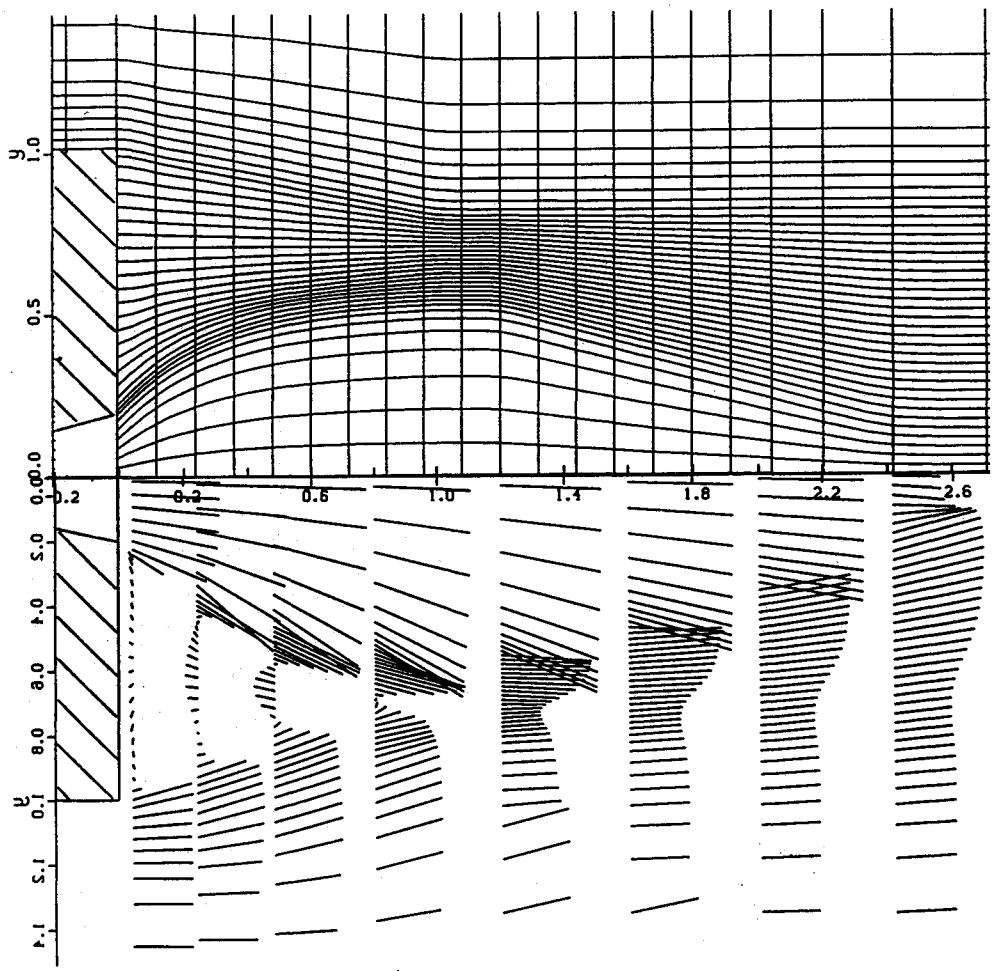

Fig. 2 Every third grid line of grid generated with the control point method and computed velocity vectors at selected stations for typical afterbody calculation.

An explicit estimate for the truncation error is obtained from the difference between Eqs. (2) and (3) and the assumption that the difference between q and q_h, the solution of the discretized differential equations L_h, is small.

$$h^n E(q_h) \simeq -L_{2h}(q_h)/(2^n - 1) \tag{4}$$

The right-hand side of Eq. (4) is easily evaluated, and it provides an estimate of the truncation error $h^n E$ associated with the solution computed with a particular grid and discretization scheme.

Figure 3 shows the grid and the computed velocity vectors in the vicinity of the nozzle lip. The vectors at $x < 0$ represent velocities imposed at the nozzle exit boundary condition. The grids differ in the alignment between the grid lines and velocity vectors (streamlines), but not in the typical grid spacing in this region. (A finite-difference plotting routine was used to display these finite-volume results. The velocity vectors should originate at the cell centers rather than the corners.) In Fig. 3a, the grid is aligned with flow exiting the nozzle, but not with the flow in the shear layer. In Fig. 3b, the grid is aligned with the flow in the shear layer, but not at the nozzle exit plane. The grid and flow could not be aligned throughout the plume with the present grid-generation method. The truncation error in the density equation from Eq. (4) is given in Fig. 4, and the largest errors occur at the corners of the base. The maximum truncation error in Fig. 4a is at a greater radius than the nozzle lip and is associated with the expansion and shear layer shown in Fig. 3a. In Fig. 4b, the majority of the error is below the lip, which is in the region of the expansion fan below the shear layer. The maximum errors occur where the solution varies and where grid lines and streamlines are not aligned.

Alignment of the grid with the streamlines in the jet shear layer, as in Fig. 3b, also eliminates the undershoot in pressure. The pressure undershoot at the nozzle lip, $r = 0.2$ in Fig. 5, occurs in the region of maximum truncation error in Fig. 4a. The undershoot does not occur when the truncation error is within the plume, as in Fig. 3b. By aligning grid lines with streamlines in the plume shear layer, solutions have been obtained at *NPR* as high as 300 for the Pegasus launch vehicle.[25]

Solutions that are nearly grid-independent have been obtained by adapting the grid to the solution and by increasing the number of grid points. Figure 6 gives the computed base pressures on a series of grids that were progressively finer and better aligned with the flow. There was no tendency for the base pressure to differ significantly, except for the undershoot, as the grid was refined. These results suggest that the truly grid-independent base pressure will not differ by more than a few percent of freestream pressure from the value computed on the finest grid in Fig. 6. This level of accuracy is adequate for virtually all design or analysis purposes.

Turbulence Modeling

Many aspects of turbulence in afterbody flows, including the effects of high Mach numbers, shear-layer curvature, merging or colliding shear layers, and shock interactions, are predicted very poorly by existing turbulence models. The

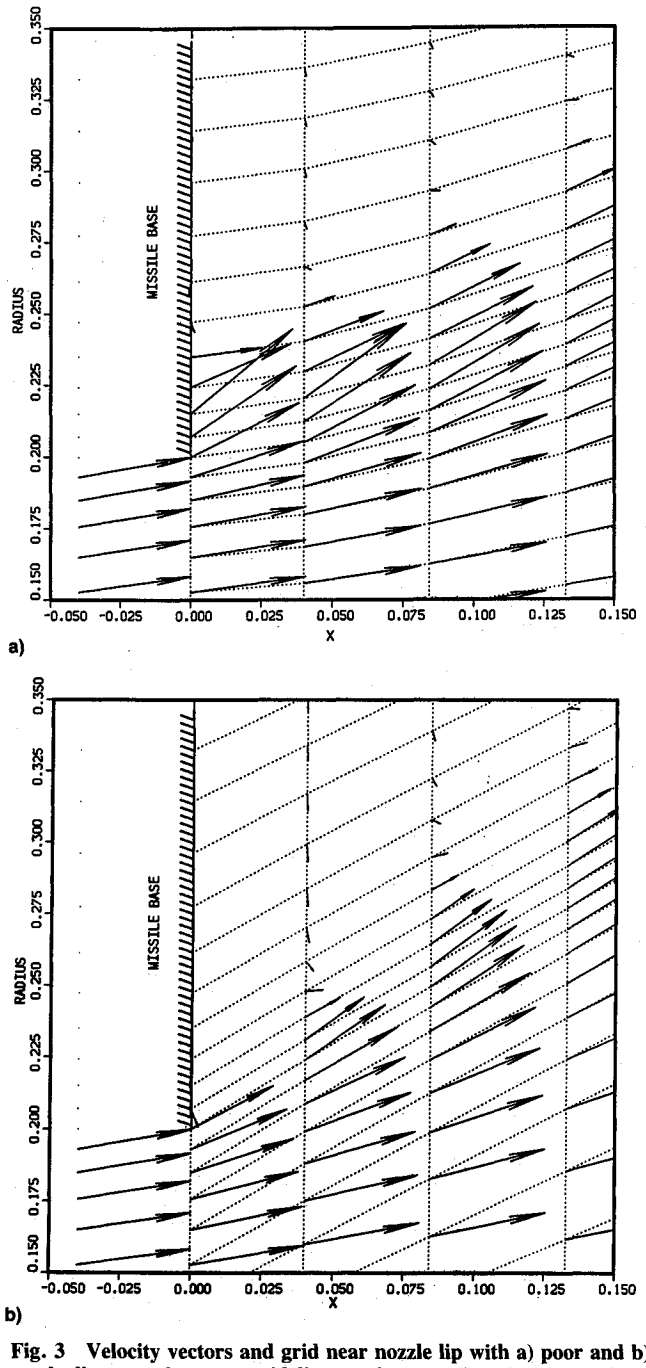

Fig. 3 Velocity vectors and grid near nozzle lip with a) poor and b) good alignment between grid lines and streamlines in plume shear layer.

Baldwin and Lomax[26] model is commonly used for missile afterbody predictions, but it was developed for thin equilibrium shear layers and predicts none of that above-mentioned phenomena. The goals of this section are to demonstrate that turbulence modeling is important in afterbody flow predictions, and that a model which accounts for Mach number and streamline curvature effects can improve prediction accuracy.

The $k-\varepsilon$ model is used as the basis of this work because it is one of the best models currently available. Turbulent stresses are computed from the Boussinesq approximation:

$$\tau_{ij} = \mu_t(\partial U_i/\partial x_j + \partial U_j/\partial x_i) - \delta_{ij}(\rho k + \mu_t \partial u_i/\partial x_i)2/3 \quad (5)$$

in which $\mu_t = c_\mu \rho k^2/\varepsilon$. The k-equation is obtained from the trace of the Reynolds-stress transport equations with an approximation for diffusive transport and the assumption that pressure-strain correlations do not alter the turbulence energy in compressible flow.

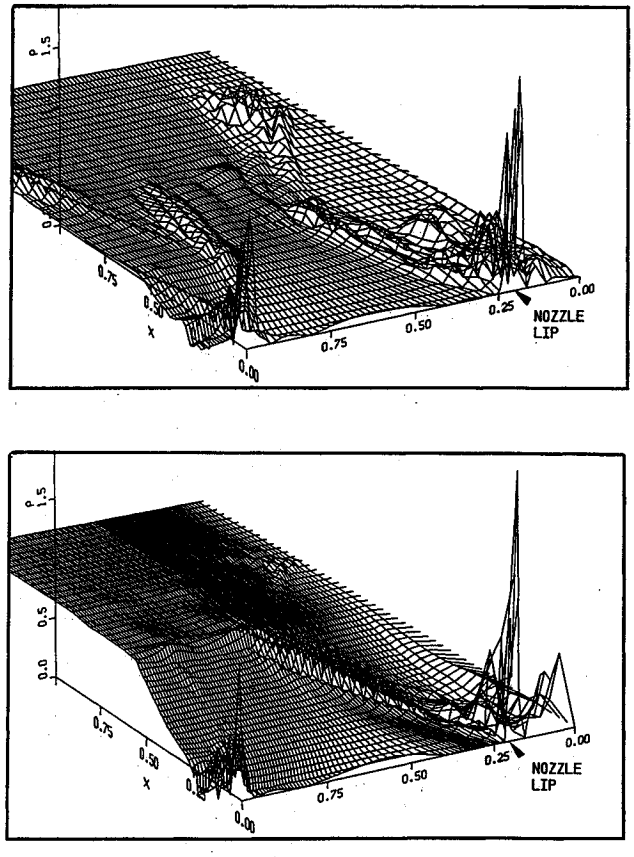

Fig. 4 Truncation error in the density equation for the entire afterbody region for grids and solutions shown in Fig. 3a and Fig. 3b.

$$\frac{D\rho k}{Dt} - \frac{\partial}{\partial x_j}\frac{\mu_t}{\sigma_k}\frac{\partial k}{\partial x_j} = P_k - \rho\varepsilon \quad (6)$$

The standard ε-equation is

$$\frac{D\rho\varepsilon}{Dt} - \frac{\partial}{\partial x_j}\frac{\mu_t}{\sigma_\varepsilon}\frac{\partial \varepsilon}{\partial x_j} = C_{\varepsilon 1}\frac{\varepsilon}{k}P_k - C_{\varepsilon 2}\frac{\rho\varepsilon^2}{k} \quad (7)$$

in which $P_k = \tau_{ij}\partial U_i/\partial x_j$ and the model coefficients are $\sigma_k = 1.0$, $\sigma_\varepsilon = 1.3$, and $C_{\varepsilon 1} = 1.45$.

In the "standard" $k-\varepsilon$ model, subsequently denoted the STD model, $C_\mu = 0.09$ and $C_{\varepsilon 2} = 1.92$. Modifications to the $k-\varepsilon$ model to account for the effects of high Mach number, streamline curvature, and both Mach number and curvature are described below, and they are denoted the M, C, and MC models, respectively. In these models, the coefficients C_μ and $C_{\varepsilon 2}$ can vary. Wall functions (e.g., Ref. 19, p. 1499) are used to compute k, ε, and the shear stress at all solid wall boundaries. Wall functions are appropriate for the flows considered since the wall-bounded flows are either wholly attached or wholly reversed, and separation occurs at the sharp base corner.

Modification for Mach Number

Compressibility effects on turbulence are significant in high-speed free shear layers. The shear stress and spreading rate $d\delta/dx$ of a plane free shear layer decrease as the Mach number difference across the layer ΔM becomes large.[27,19] For incompressible flow, $d\delta/dx \simeq 0.115$, but this drops to $d\delta/dx \simeq 0.03$ for $\Delta M = 5$. Morkovin[28] argued that compressibility effects become important as the velocity of turbulent fluctuations approaches the sonic speed; hence, Mach-number effects depend on a Mach number of the turbulent fluctuations $k^{1/2}/a$. A considerable amount of recent work (e.g., Ref. 29) suggests that the reduced growth rate of instability modes at higher

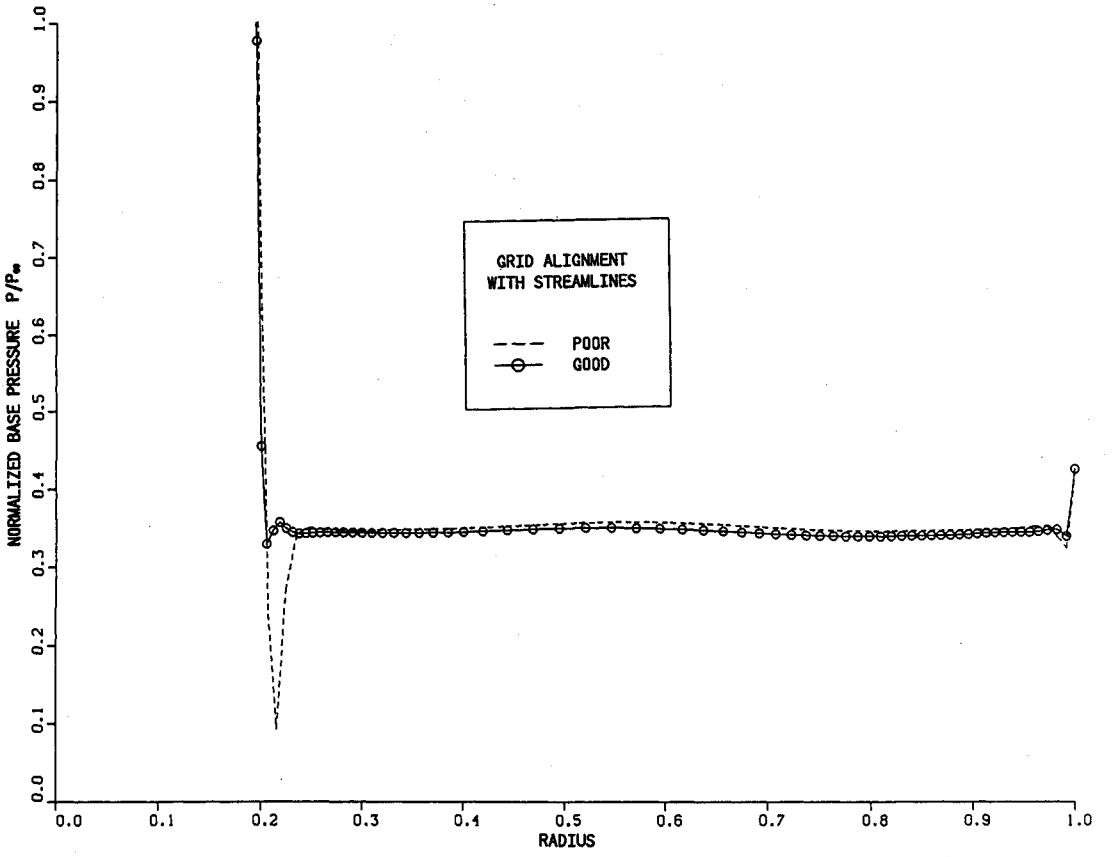

Fig. 5 Base pressures computed on grids in Fig. 3.

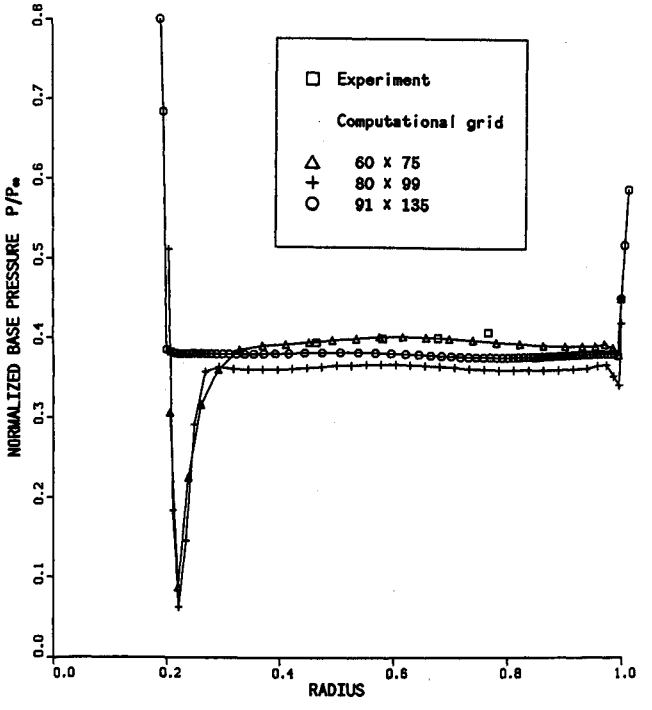

Fig. 6 Base pressures computed in a sequence of refined and improved grids.

speeds causes the reduced shear-layer growth, while other theories[30,31] have also been proposed.

The model employed here is derived from work by Bonnet (Ref. 19, p. 1408) in which fluctuations of velocity and thermodynamic quantities were related, and a compressibility correction to the pressure-strain closure model was derived. A single coefficient was empirically optimized, and the model gave good results for shear layers up to $\Delta M \sim 7$. Bonnet's model is reduced to an equilibrium form compatible with the $k-\varepsilon$ model by assuming that the flow involves homogeneous shear and that the ratio of turbulence energies in the streamwise fluctuations to all fluctuations is 0.48, which is an average of this parameter for isotropic turbulence and uniform low-speed shear flow. The model that emerges is a modification of C_μ given by

$$C_\mu = C_{\mu 0}(1 + C_{m1}k/a^2)/(1 + C_{m2}k/a^2)^2 \qquad (8)$$

in which $C_{m1} = 8.4$ and $C_{m2} = 6.5$, and $C_{\mu 0} = 0.09$. It is noteworthy that the only optimization against experimental data done in deriving Eq. (8) was that performed by Bonnet.

The effect of Eq. (8) is assessed by computing the spreading rate of a planar mixing layer with stagnant fluid on one side and a nominal density ratio across the shear layer of unity. Figure 7 compares the computed and experimental values of $d\delta/dx$ for $M \leq 5$, where the shear-layer thickness δ is the distance between the points at which the $(U/U_\infty)^2 = 0.1$ and 0.9. The computed spreading rate falls slightly below the experimental value at $M \to 0$, which is consistent with the known behavior of the $k-\varepsilon$ model[19] for this flow. As the Mach number increases, the predicted spreading rate decreases, but somewhat more slowly than the measured rate. The net result is a reasonably accurate prediction of spreading rate for $M \leq 5$.

Modification for Streamline Curvature

Streamline curvature is also expected to affect turbulence in afterbody flows, as discussed in the Introduction. Curvature effects result from at least two mechanisms. Additional rates of strain introduced by curvature alter the magnitude of turbulence production and affect turbulent stresses. This phenomenon is treated accurately if the production term P_k is complete and the stresses are accurately predicted. Curvature effects are also caused by the centrifugal "force" in a curved

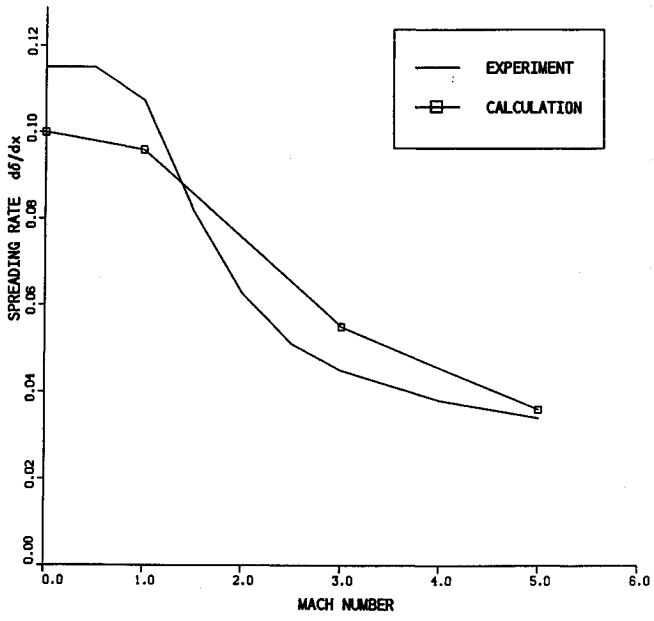

Fig. 7 Spreading rate of a plane free shear layer as a function of Mach-number difference across the shear layer; present calculations and experiment (Ref. 19, pp. 364–368).

turbulent shear layer, which affects the correlation between streamwise and normal velocity fluctuations.

At the heart of the curvature model is a stability parameter that determines if the curvature is stabilizing, which suppresses turbulence, or if it is destabilizing, which promotes turbulence. The stability parameter of a line vortex was determined by Rayleigh[32] to be $\beta = \partial r^2 V_\theta^2/\partial r$, in which r is equal to the streamline radius of curvature and V_θ is the swirl velocity. The curvature effects are stabilizing if $\beta > 0$, destabilizing if $\beta < 0$, and neutral if $\beta = 0$. An alternate stability parameter can be derived by using the Euler n-equation, $\partial p/\partial n = \rho V_\theta^2/r$, to eliminate explicit dependence on the radius of curvature:

$$\beta^* = \frac{\beta}{r^3} = \frac{1}{\rho^2 V^2}\frac{\partial p}{\partial n}\frac{\partial p_0}{\partial n} \tag{9}$$

in which V is the velocity magnitude, p is an effective pressure (thermodynamic pressure + $2\rho k/3$), $p_0 = p + \rho V^2/2$ is the incompressible total pressure, and n is normal to streamlines. Equation (9) and an alternate form $\beta^* = \nabla p \cdot \nabla p_t/(\rho V)^2$ were considered in the present work. The latter has the philosophical and computational advantages in that it is independent of mean streamlines and is applicable in three-dimensional flow. The two forms give similar values of β^* in most regions but differ somewhat at shocks. This stability parameter is appropriate for compressible and incompressible flow. Equation (9) is used for the results presented herein.

A curvature model that mimics physical processes is needed. Some evidence suggests that curvature affects the pressure-strain correlation in the Reynolds-stress equations. Gillis and Johnston[33] studied flow over a convex surface (stabilizing curvature) and observed that shear stresses were reduced rapidly while turbulence energy was reduced more slowly. Measurements indicated that the net production of shear stress was nearly zero, and "diffusion" could not cause this rapid reduction of shear stress; the pressure-strain term is the only other likely cause of this change. Also, the rapid decrease in shear stress accompanied by a smaller change in energy, which could be due to dissipation, is consistent with the properties of the pressure-strain term. Other evidence comes from the large eddy simulation of the VTOL upwash fountain by Childs and Nixon,[34] in which the pressure-strain term for shear stress was found to be dominant in the regions of high curvature and less significant elsewhere.

Equating the Reynolds-stress transport equation for shear stress to an equation for the rate of change of shear stress derived from the Boussinesq approximation Eq. (5) yields an ε-equation similar to Eq. (7), but which contains a source term involving the pressure-strain term. This process could be carried further to yield an "equilibrium" model in which curvature effects would be instantaneous. However, curvature effects do not occur instantaneously except in cases of impulsive curvature, and an equilibrium model seems inappropriate.

The model modification employed here is similar to that of Launder et al.[35] A source term that is a function of the stability parameter is added to the ε-equation by modifying $C_{\varepsilon 2}$ as follows:

$$C_{\varepsilon 2} = C_{\varepsilon 20} f_c, \qquad f_c = \left(1 - C_c \frac{k^2}{\varepsilon^2}\beta^*\right) \tag{10}$$

in which $C_{\varepsilon 20} = 1.92$ is the value of $C_{\varepsilon 2}$ when streamline curvature is negligible, and C_c is the curvature model coefficient.

Launder selected $C_c = 0.2$ for computing flow over spinning cones. Rodi and Scheuerer[36] found that $C_c = 0.25$ overpredicted curvature effects slightly in two stabilized shear flows and by roughly 100% in a destabilized flow. Bradshaw[20] has noted that stabilizing and destabilizing curvature affects turbulence quite differently and may need to be modeled differently. From the above results, the following values for C_c are selected for stabilized and destabilized curvature:

$$C_c = \begin{cases} 0.2 & \text{for } \beta > 0 \\ 0.1 & \text{for } \beta < 0 \end{cases} \tag{11}$$

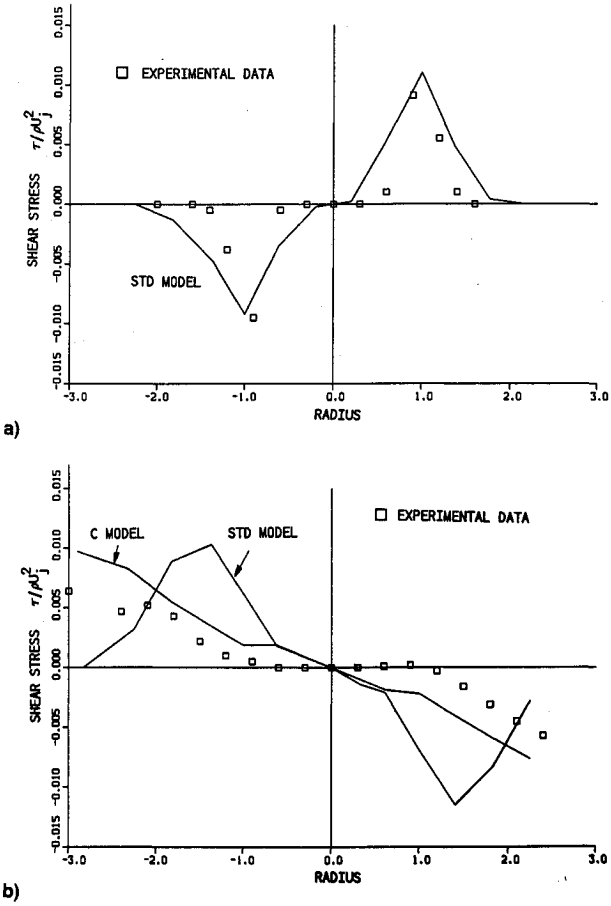

Fig. 8 Comparison of measured[37] and computed shear stresses in a) free jet and b) impingement regions of an impinging turbulent jet.

As with the Mach-number modification, the values of the model coefficient are based on results from other researchers for flows not related to afterbody flows.

Limits on f_c and on V in the denominator of Eq. (9) are imposed to suppress erratic model behavior at stagnation points and in regions of very high curvature, such as shocks: $0.1 \leq f_c \leq 2.0$ and $V \geq 0.1\, V_{\text{ref}}$ where the reference velocity is taken to be the freestream velocity. A suitable means of eliminating the need for these limits was sought but was not found. Predicted results can be sensitive to these limits. For example, the ε-equation is unstable if $f_c < 0$. Further work is needed in this area.

Calculations were performed of an incompressible circular jet impinging normally on a plate to assess the accuracy of the C model in the impingement zone where the flow experiences rapid turning. Figure 8 shows the shear stress computed with the STD model in the free jet region, and agreement with measurements[37] is good. Results from the STD and C models are virtually identical and were not plotted separately. In the impingement zone, the STD model gives very poor accuracy and overpredicts the shear stress by an enormous margin. Barata et al.[38] have noted comparable accuracy from the STD model in a similar flow. The accuracy of the C model in this calculation is perhaps only adequate, as shown in Fig. 8, but it is a large improvement over the STD model.

Turbulence Model Effects in Afterbody Flows

The effects on high-speed afterbody flow predictions of the above modifications to the $k-\varepsilon$ model are examined. Figure 9 shows the base pressures for the $NPR = 2.15$ case of Petrie and Walker.[16] Results from the STD and MC models are close to the experimental data, and, based on these results alone, it would be inappropriate to consider one model superior to the other. The M and C models predict the base pressure to be higher and lower than the experimental data, respectively. The changes in base pressure caused by Mach-number and curvature effects correspond to variations of +22 and −14% in base drag, respectively. The good base pressure prediction of the STD model results from fortuitous cancellation of errors of opposite sign caused by the STD model's poor accuracy for both Mach-number and curvature effects.

Figure 10a gives a comparison of the experimental shadowgraph and the Mach-number contours predicted with the MC model. In the shadowgraph, the plume shear layer, the outer shear layer, Mach disk, and the recompression are visible, and agreement with the calculation is good. The Mach-number contours also show a barrel shock that is absent in the shadowgraph. A comparison of the velocity field is presented in Fig. 10b, and generally good agreement is again

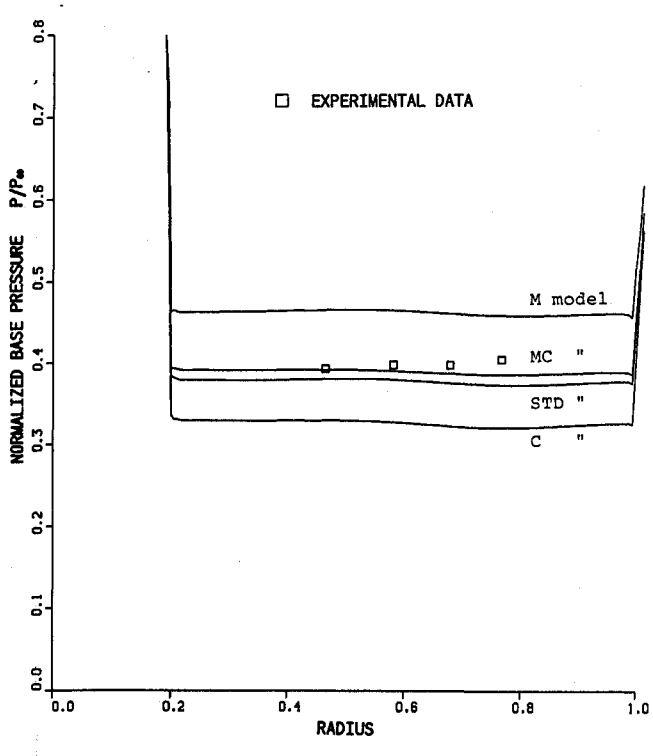

Fig. 9 Base pressures for the $NPR = 2.15$ case of Petrie and Walker[16] computed with four variations of the $k-$ model. Symbols denote experimental data.

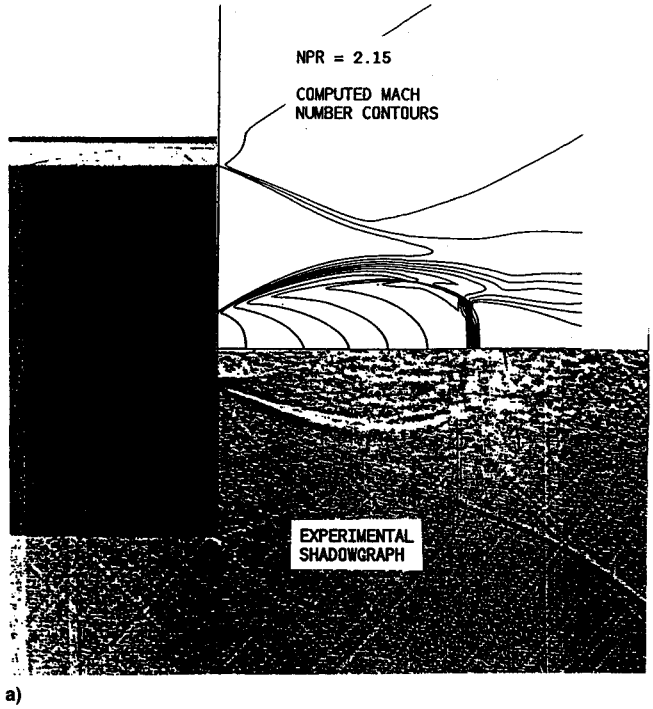

a)

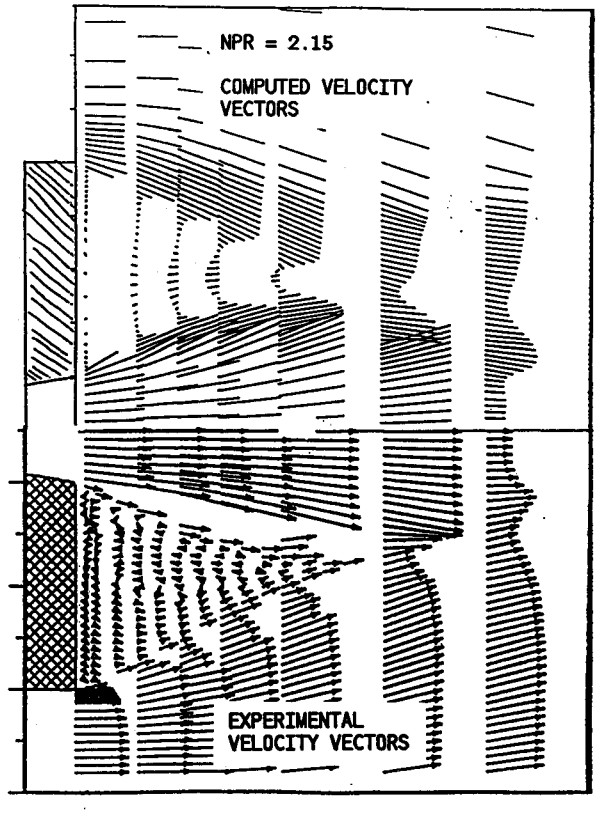

b)

Fig. 10 Comparison of a) shadowgraph and computed Mach-number contours, and b) measured and computed velocity vectors for the $NPR = 2.15$ case of Petrie and Walker[16] computed with the MC model.

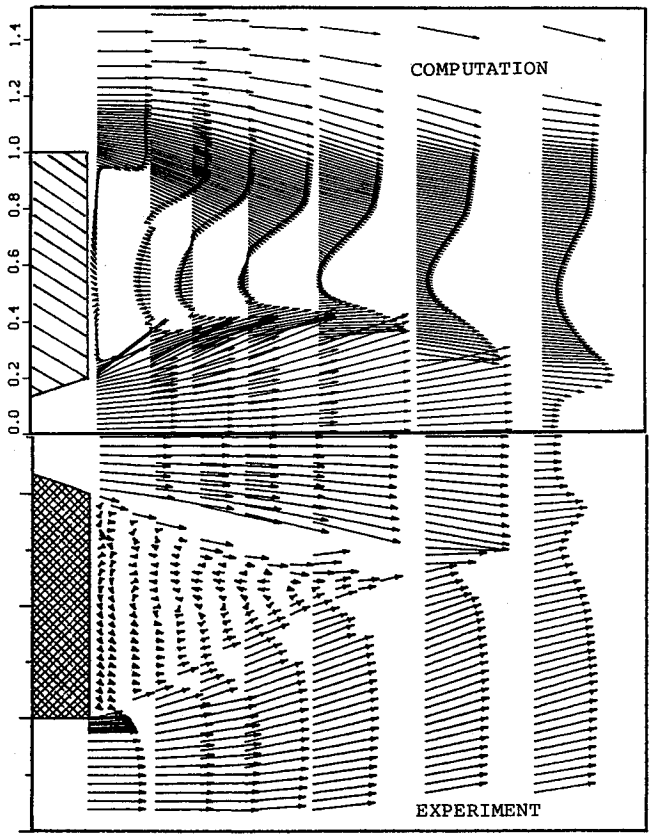

Fig. 11 Velocity vectors predicted by the STD model for the *NPR* = 2.15 case of Petrie and Walker.[16]

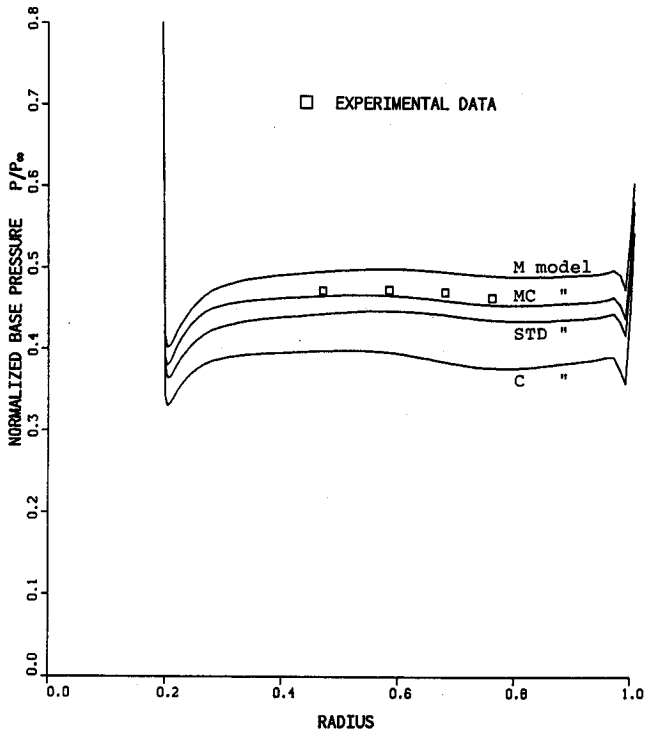

Fig. 12 Base pressures for the *NPR* = 6.44 case of Petrie and Walker[16] computed with four variations of the $k-$ model. Symbols denote experimental data.

seen. In particular, the predicted extent of reversed flow is nearly correct. There are also some significant differences between experiment and computation. The location of the center of the recirculation is poorly predicted. The recirculation pattern can affect base heating rates and the effectiveness of modifications to the base shape for increasing vehicle performance. In the farthest downstream line of velocity vectors, the predicted velocities display slightly greater variation than do the experimental data.

Figure 11 gives velocity vectors predicted by the STD model, and the accuracy is poor. This shows that base pressure alone is not a good diagnostic of a method's accuracy. Comparison with velocities given by the STD and MC models provides more evidence that Mach-number and curvature effects are important in these flows.

Figure 12 gives the base pressures for the *NPR* = 6.44 case of Petrie and Walker[16] computed with the different models. The trends are qualitatively similar to the *NPR* = 2.15 case. The results from the STD and MC models differ only slightly and are close to the measurements, while the results from the M and C models differ significantly from the STD model. In this case, the effects of the curvature modification are greater than in the *NPR* = 2.15 case, while Mach-number effects are smaller. Excellent agreement between the computed Mach-number contours and the experimental shadowgraph is shown in Fig. 13a. The computed and measured velocity vectors are shown in Fig. 13b and, while there is generally good agreement, some discrepancies are present. The most significant of these may be in the pattern and magnitude of velocities in the reverse flow region. There are also differences in the area just downstream of the barrel shock and Mach disk. Measurements were made with laser velocimetry, and errors due to particle lag may contribute to this discrepancy.

Summary and Conclusions

An implicit finite-volume Navier-Stokes prediction method has been used to compute missile afterbody flows. The method is second-order accurate and employs a characteristic upwind scheme for inviscid terms which has good shock-capturing abilities. A $k-\varepsilon$ model is used to predict the effects of turbulence. The objectives of the work were to identify and to reduce or eliminate the dominant sources of error in afterbody flow calculations.

The effects of discretization accuracy were evaluated using a method to estimate truncation error. It was shown that discretization accuracy can be increased significantly by aligning grid lines and streamlines in regions of large solution gradients. So aligning the grid made it possible to obtain solutions at high nozzle pressure ratios and appears to eliminate the computational problem associated with highly underexpanded jets. Solutions with negligible grid dependence in the dominant flow features were obtained.

Modifications to the $k-\varepsilon$ model to account for Mach-number and streamline curvature effects on turbulence were described. The accuracy of these modifications was demonstrated by other researchers against generic turbulence experiments unrelated to afterbody flows. Separately, the curvature and Mach-number modifications produce significant changes in afterbody flowfields corresponding to changes in base drag in excess of 20%, for the flows considered here. It is inferred that Mach-number and curvature effects on turbulence play a significant role in determining global afterbody flow characteristics. Comparisons with experiment indicate that the inclusion of the Mach-number and curvature modifications significantly improves the accuracy of the $k-\varepsilon$ model.

The need for further research in two areas is indicated by this work. One area is the development of a grid-generation procedure that causes grid lines to follow streamlines in regions of large solution gradients. The other involves turbulence modeling in regions of large or impulsive curvature, such as, at stagnation points, through shocks, and in vortex cores.

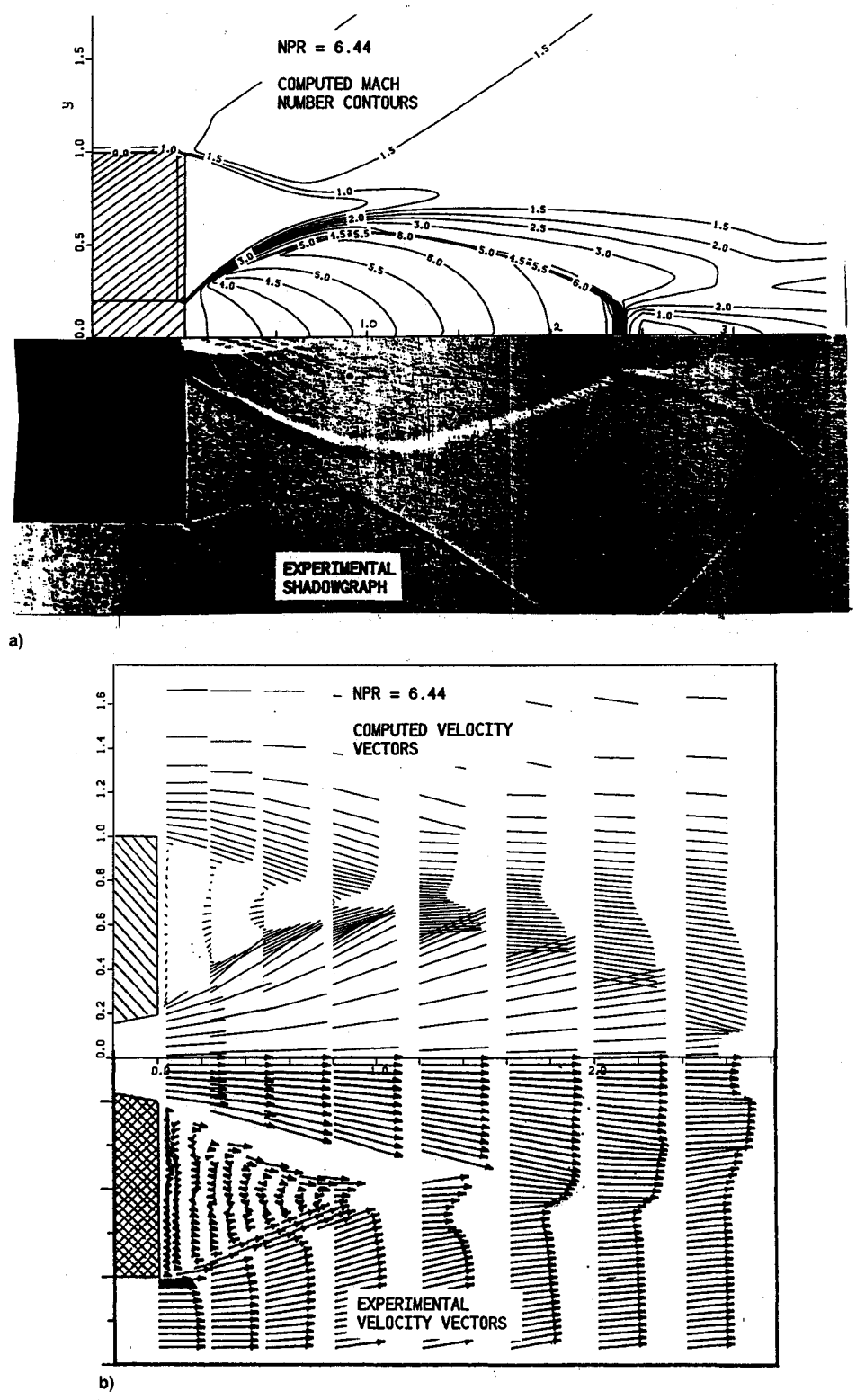

Fig. 13 Comparison of a) shadowgraph and computed Mach-number contours, and b) measured and computed velocity vectors for the *NPR* = 6.44 case of Petrie and Walker[16] computed with the MC model.

Acknowledgments

The authors gratefully acknowledge the support of the Army Research Office through Contract DAAL03-86-C-0002 and the NASA/Ames Research Center for access to computational facilities. Support for the impinging jet calculations was provided by the Flight Dynamics Laboratory at the Wright Research and Development Center under Contract F33615-88-C-3020. Appreciation is extended to Dr. Coakley of NASA/Ames Research Center for the use of the TURF computer code.

References

[1]Korst, H. H., Page, R. H., and Childs, M. E., "A Theory for Base Pressure in Transonic and Supersonic Flows," Univ. of Illinois, Dept. of Mechanical and Industrial Engineering, Rept. ME-TN-392-2, March 1955.

[2]Putnam, L. E., and Hodges, J., "Assessment of NASA and RAE Viscous-Inviscid Interaction Methods for Predicting Transonic Flow Over Nozzle Afterbodies," AIAA Paper 83-1789, July 1983.

[3]Holst, T. L., "Numerical Solution of Axisymmetric Boattail Fields with Plume Simulators," AIAA Paper 77-0224, Jan. 1977.

[4]Mikhail, A. G., "Computation of Supersonic Flow Past an Axi-

symmetric Nozzle Boattail with Jet Exhaust," AIAA Paper 78-0993, July 1978.

[5]Deiwert, G. S., Andrews, A. E., and Nakahashi, K., "Theoretical Analysis of Aircraft Afterbody Flow," *Journal of Spacecraft*, Vol. 24, No. 6, 1987, pp. 496–503.

[6]Beam, R., and Warming, R. F., "An Implicit Finite-Difference Algorithm for Hyperbolic Systems in Conservation-Law Form," *Journal of Computational Physics*, Vol. 22, Sept. 1976, pp. 87–110.

[7]Sahu, J., and Nietubicz, C. J., "Numerical Computation of Base Flow for a Missile in the Presence of a Propulsive Jet," AIAA Paper 84-0527, Jan. 1984.

[8]Lombard, C. K., Luh, R. C.-C., Nagaraj, N., Bardina, J., and Venkatapathy, E., "Numerical Simulation of Backward Step and Jet Exhaust Flows," AIAA Paper 86-0432, Jan. 1986.

[9]Hoffman, J. J., Birch, S. F., and Hopcraft, R. G., "Navier-Stokes Calculations of Rocket Base Flows," AIAA Paper 87-0466, Jan. 1987.

[10]Thomas, P. D., Reklis, R. P., Roloff, R. R., and Conti, R. J., "Numerical Simulation of Axisymmetric Base Flow on Tactical Missiles with Propulsive Jet," AIAA Paper 84-1658, June 1984.

[11]Launder, B. E., and Spaulding, D. B., *Mathematical Models of Turbulence*, Academic Press, London, and New York, 1972.

[12]Launder, B. E., and Spaulding, D. B., "The Numerical Computation of Turbulent Flows," *Computer Methods in Applied Mechanics and Engineering*, Vol. 3, 1974, pp. 169–189.

[13]Fox, J. H., "Predicting Plume-Induced Separation on Bluff-Based Bodies," AIAA Paper 84-0315, Jan. 1984.

[14]Venkatapathy, E., and Lombard, C. K., "Accurate Numerical Simulation of Jet Exhaust Flows with CSCM for Adaptive Overlapping Grids," AIAA Paper 87-0465, Jan. 1987.

[15]Putnam, L. E., and Bissinger, N. C., "Results of AGARD Assessment of Prediction Capabilities for Nozzle Afterbody Flows," AIAA Paper 85-1464, July 1985.

[16]Petrie, H. L., and Walker, B. J., "Comparison of Experiment and Computation for a Missile Base Region Flowfield with a Centered Propulsive Jet," AIAA Paper 85-1618, July 1985.

[17]Childs, R. E., and Caruso, S. C., "On the Accuracy of Turbulent Base Flow Predictions," AIAA Paper 87-1439, June 1987.

[18]Caruso, S. C., and Childs, R. E., "Aspects of Grid Topology for Reynolds-Averaged Navier-Stokes Base Flow Calculations," AIAA Paper 88-0523, Jan. 1988.

[19]Kline, S. J., Cantwell, B. J., and Lilley, G. M. (eds.), *The 1980-81 AFOSR-HTTM-Stanford Conference on Complex Turbulent Flows*, Stanford University, CA, 1981.

[20]Bradshaw, P., "Effects of Streamline Curvature on Turbulent Flow," AGARDograph No. 169, Aug. 1973.

[21]Coakley, T. J., "Implicit Upwind Methods for the Compressible Navier-Stokes Equations," *AIAA Journal*, Vol. 23, No. 3, 1985, pp. 374–380.

[22]Eiseman, P. R., "A Control Point Form of Algebraic Grid Generation," *International Journal for Numerical Methods in Fluids*, Vol. 8, Oct. 1988, pp. 1165–1181.

[23]Klopfer, G. H., "Solution Adaptive Meshes with a Hyperbolic Grid Generator," *Numerical Grid Generation in Computational Fluid Mechanics*, edited by S. Sengupta, Haüser, J., Eiseman, P. R., and Thompson, J. F., Pineridge Press Limited, Swansea, 1988, pp. 443–454.

[24]Berger, M. J., and Jameson, A., "Automatic Adaptive Grid Refinement for the Euler Equations," *AIAA Journal*, Vol. 23, No. 4, 1985, pp. 561–568.

[25]Mendenhall, M. R., Lesieutre, D. J., Caruso, S. C., Dillenius, M. F. E., and Kuhn, G. D., "Aerodynamic Design of Pegasus™ Concept to Flight with CFD," AGARD Symposium on Missile Aerodynamics, Friedrichshafen, Federal Republic of Germany, April 1990.

[26]Baldwin, B. S., and Lomax, H., "Thin-Layer Approximation and Algebraic Model for Separated Turbulent Flows," AIAA Paper 73-0257, Jan. 1973.

[27]Birch, S. F., and Eggers, J. M., "A Critical Review of the Data for Developed Free Turbulent Shear Layers," NASA SP-321, Vol. 1, 1972, pp. 11–40.

[28]Morkovin, M. V., "Effects of Compressibility on Turbulent Flow," Symposium International de la Mechanique Turbulence, Centre Nat. de la Rech. Sci. Paris, France, 1962, pp. 367–380.

[29]Sandham, N., and Reynolds, W. C., "The Compressible Mixing Layer: Linear Theory and Direct Simulation," AIAA Paper 89-0371, Jan. 1989.

[30]Nixon, D., Keefe, L. R., and Kuhn, G. D., "The Effects of Compressibility on a Supersonic Mixing Layer," AIAA Paper 90-0706, Jan. 1990.

[31]Zeman, O., "Dilatation Dissipation: The Concept and Application in Modeling Compressible Mixing Layers," *Physics of Fluids A*, Vol. 2, No. 2, 1990, pp. 178–188.

[32]Rayleigh, Lord, "On the Dynamics of Revolving Fluids," *Proceedings of the Royal Society*, Vol. 93, 1916, p. 193.

[33]Gillis, J. C., and Johnston, J. P., "Turbulent Boundary-Layer Flow and Structure on a Convex Wall and its Redevelopment on a Flat Wall," *Journal of Fluid Mechanics*, Vol. 135, 1983, pp. 123–153.

[34]Childs, R. E., and Nixon, D., "Unsteady Three-Dimensional Simulations of a VTOL Upwash Fountain," AIAA Paper 86-0212, Jan. 1986.

[35]Launder, B. E., Priddin, C. H., and Sharma, B. I., "The Calculation of Turbulent Boundary Layers on Spinning and Curved Surfaces," *Transactions of the ASME, Journal of Fluids Engineering*, March 1977, pp. 231–239.

[36]Rodi, W., and Scheuerer, G., "Calculation of Curved Shear Layers with Two-Equation Turbulence models," *Physics of Fluids*, Vol. 26, No. 6, 1983, pp. 1422–1436.

[37]Saripalli, K. R., "Laser Doppler Velocimeter Measurements in a 3-D Impinging Twin-Jet Fountain Flow," AIAA Paper 85-4036, Oct. 1985.

[38]Barata, J. M. M., Durão, D. F. G., and McGuirk, J. J., "Numerical Study of Single Impinging Jets Through a Crossflow," AIAA Paper 89-0449, Jan. 1989.